Determination of intrinsic kinetic parameters in photocatalytic multi-tube reactors by combining the $NTU_m - method$ with radiation field modelling

Determination of intrinsic kinetic parameters in photocatalytic multi-tube reactors by combining the NTU_m-method with radiation field modelling

Jeroen van Walsem[†‡], Jelle Roegiers[†‡], Bart Modde[§], Silvia Lenaerts[†], Siegfried Denys[†,]*

† Sustainable Energy, Air & Water Technology, Department of Bioscience Engineering, University of Antwerp, Groenenborgerlaan 171, B-2020 Antwerp, Belgium.

§ Vento Ltd., Bedrijvenpark Coupure 5, B-9700 Oudenaarde, Belgium.

* E-mail: Siegfried.Denys@uantwerp.be

Fax: +32 3 265 32 25. Tel: +32 3 265 32 30.

‡ These authors contributed equally.

Keywords

Intrinsic kinetic parameters; NTU_m-method; Photocatalysis; Radiation field modelling; Multi-tube reactor

Highlights

- NTU_m–method adapted for a photocatalytic multi-tube reactor
- Insights in the reaction rate limiting behavior of a photocatalytic multi-tube reactor
- Extended NTU_m–method, including radiation field modelling, for intrinsic kinetic parameter determination
- Outstanding agreement between predicted and experimental reactor outlet concentrations

1. Abstract

In this work, we propose an adapted Number of Transfer Units (NTU_m)-method as an effective tool to determine the Langmuir-Hinshelwood kinetic parameters for a photocatalytic multi-tube reactor. The Langmuir-Hinshelwood rate constant k_{LH} and the Langmuir adsorption constant K_L were determined from several experiments under different UV-irradiance conditions, resulting in irradiance depending values for k_{LH}. In order to determine a unique, intrinsic empirical constant k_0, valid for all irradiation conditions, we coupled the adapted NTU_m-method with a radiation field model to predict UV-irradiance distribution inside the reactor. The final set of kinetic parameters were derived using a Generalized Reduced Gradient (GRG) nonlinear solving method in Matlab which minimizes the differences between model and experimental reactor outlet concentrations of acetaldehyde for various photocatalytic experiments under varying operating conditions, including inlet concentration, flow rate and UV-irradiance. An excellent agreement of the intrinsic empirical constant k_0, derived from the coupled NTU_m-radiation field model and an earlier published CFD approach was found, emphasizing its validity and reliability.

2. Introduction

Volatile organic compounds (VOCs) are recognized as one of the major indoor air contaminants, emitted from building materials or human activities such as smoking, cleaning or heating. VOCs are present at low ppb concentrations in indoor air, but are known to cause the Sick Building Syndrome (SBS) which comprises various acute health and comfort effects that appear to be linked to time spent in a building [1,2]. In this work, acetaldehyde, a typical VOC in indoor air, was taken as model component. Acetaldehyde is commonly reported in all kinds of buildings, with concentrations around 90 ppbv [3]. Specific indoor air sources for acetaldehyde are glues, paints, deodorants and fuel additives [4,5]. Nowadays, buildings are

tightened up by heat-insulation measurements which decrease (natural) fresh air supply and cause pollutant accumulations [6]. For this reason, the indoor VOC concentrations are actually higher than in the outdoor environment [7]. Significant energy savings can be achieved by reducing ventilation rates, but in order to prevent VOC accumulation, air cleaning systems have to compensate for the diminished pollutant removal by ventilation. For instance, to achieve 50% reduction in air ventilation that contains 15-20% outdoor air and 80-85% re-circulated indoor air, a single-pass removal efficiency of 15-20% is required [8]. Traditional air filtration is unable to deal with gaseous components, whereas suitable cleaning technologies, such as active carbon adsorption, require thermal energy for regeneration of the adsorptive medium [9,10]. Photocatalytic oxidation (PCO) proved to be a promising technique for indoor air purification [11–13]. Still, the gap between operational lab-scale photocatalytic reactors and commercialized reactors is not resolved [9]. Partially, this can be explained because realistic conditions are totally different from the typical conditions in experimental setups (as in this work, often much higher pollutant concentrations and low flow rates are used in lab-scale experiments due to practical limitations) [14]. Therefore, the urging need for reliable intrinsic kinetics and design methods is clearly stated in literature [15–18]. Intrinsic parameters should be independent of fluid dynamics, reactor geometry and radiation field [9]. An analytic approach based on an analogy between heat transfer and mass transfer, the Number of Transfer Units (NTU_m)-method, was proposed by Zhang et al. [19,20] as an effective method for determining the intrinsic Langmuir-Hinshelwood (LH) kinetic parameters, as well as a useful tool for reactor design. In earlier research, we have proven the usefulness of their method by accurately determining the kinetic parameters (the LH reaction rate constant and the Langmuir adsorption constant), in a slit-shaped flat bed photocatalytic reactor [21]. The drawback of this approach is its transferability to other reactor geometries or irradiation conditions. In this work, we propose an enhanced version of the original analytic approach by Zhang et al. [18,19], able

to derive the intrinsic kinetic parameters of a photocatalytic multi-tube reactor, independent of pollutant concentration, fluid flow and radiation field. The proposed method is based on combining the NTU_m-method with a UV radiation field model.

3. Methodology

3.1 Reactor and experimental setup

Continuous flow experiments were conducted with a small, lab scale multi-tube reactor, as extensively described in previous work [22–24]. Seven coated borosilicate glass tubes (7.0 mm inner diameter, 9.0 mm outer diameter and 240 mm length) were placed in the center of a borosilicate housing (29 mm inner diameter) as shown in Figure 1.

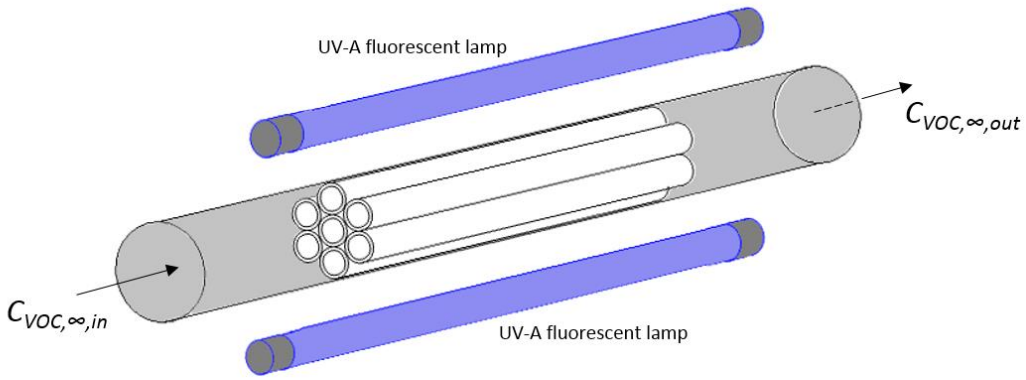

Figure 1: Schematic representation of the lab scale multi-tube reactor

The coating procedure, consisting of a 0.5 M solution of commercial titanium isopropoxide (TTIP, 97 %, Aldrich), isopropanol (i-PrOH, Sigma- Aldrich), diethanolamine (DEA, Sigma-Aldrich) (with a DEA/TTIP molar ratio of 4 and a H_2O/TTIP molar ratio of 2) and 10 g/L P25 TiO_2 (Evonik), is similar to the P25 based powder-modified sol-gel method described by Chen et al. [25,26]. The photocatalytic coating was applied using a dip-coating device (Bungard Elektronik, RDC21-K) with a fixed withdrawal speed of 120 mm min^{-1} and dried afterwards at

room temperature for 24 hours. Both the inside and the outside of the tubes were coated during the same dip-coating procedure. A subsequent calcination step at 500°C for 1 hour was required to finalize the immobilization. Two UV-A fluorescent lamps (Sylvania F8W/BLB-T5) were positioned on opposite sides of the reactor (Figure 1), at varying distance (20, 40 and 60 mm), resulting in three irradiation conditions. Each setup or distance corresponds to a certain irradiance condition. The experiments were performed with a fully automated setup which is described in detail by Tytgat et al. [27]. Acetaldehyde (Messer, 1% in N_2) was mixed with synthetic clean air (Messer) using mass flow controllers allowing a broad inlet concentration range of 8-60 ppm(v) at a total gas flow rate range of 500–2000 cm^3 min^{-1}. At least 15 different operating conditions (determined by a certain mass flow rate and VOC concentration) were tested for each of the three irradiance conditions. As in previous work, the outlet acetaldehyde concentration was measured using online FTIR spectroscopy (ν(C-H) stretch vibration corresponding to an IR peak height at 2728 cm^{-1}) [22,28]. In all the experiments, the relative humidity and temperature of the gas stream was kept at 5% and 20°C respectively, as this has been established in earlier research as appropriate conditions for obtaining reliable and reproducible measurements [21].

3.2 Reaction kinetics

In the literature, the Langmuir-Hinshelwood (LH) rate equations have often been used to successfully describe the photocatalytic gas phase reactions [29–31]. In this work, a monomolecular LH model was assumed which excludes by-products and intermediates formation (and thus adsorption competition), to obtain simplified rate expressions. Li Puma et al. (2009) observed that possible reaction products do not influence the observed oxidation rates [18]. In earlier work, we have clearly shown the accuracy of the LH mechanism to describe acetaldehyde adsorption and degradation phenomena using both analytic and CFD approaches [21,24]. The photocatalytic reaction rate (r) is commonly written as (eq. 1):

$$r = k_{LH}\theta_{VOC} = \frac{k_{LH}K_L C_{VOC}}{1+K_L C_{VOC}} = k_{app} C_{VOC} \quad \text{(eq. 1)}$$

With θ_{VOC} the fractional coverage, k_{LH} the Langmuir-Hinshelwood rate constant [mol m^{-2} s^{-1}], K_L the Langmuir adsorption constant under irradiation ($\equiv k_{adsorption}/k_{desorption}$) [$m^3$ mol^{-1}], C_{VOC} the acetaldehyde concentration in close proximity of the photocatalytic surface which should not be confused with the bulk VOC concentration [mol m^{-3}] and k_{app} the apparent reaction rate coefficient [m s^{-1}]. In general, the Langmuir-Hinshelwood rate constant depends on the UV light irradiance, often expressed by the following relation (eq. 2) [32]:

$$k_{LH}(I) = \begin{cases} k_0 I, & I < 10\ W/m^2 \\ k_0\sqrt{I_0 I} & I > 10\ W/m^2 \end{cases} \quad \text{(eq. 2)}$$

With k_0 an intrinsic, empirical constant, I_0 a threshold value of 10 W m^{-2} and I the intensity of UV light [W m^{-2}].

3.3 Mass transfer based model (NTU_m-method) adapted for a multi-tube reactor

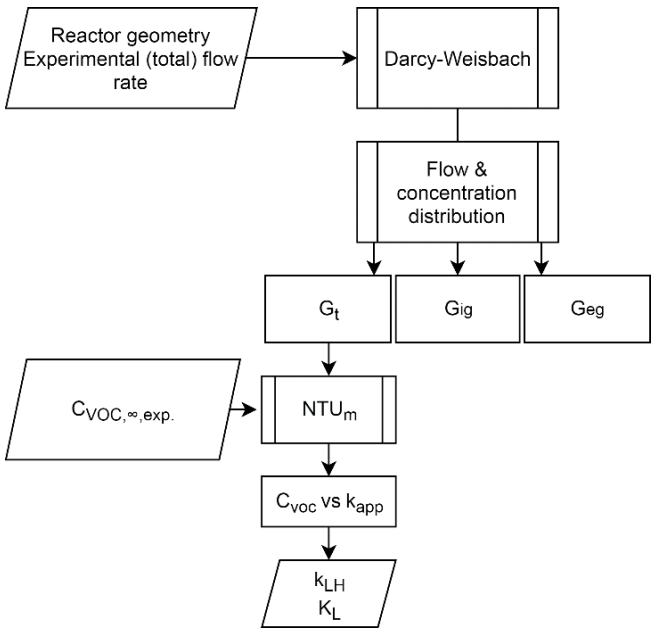

Figure 2: Overview of the methodology of the mass transfer based model (NTU_m-method), adapted for a multi-tube photocatalytic reactor

3.3.1 Flow and concentration distribution

In the particular case of the multi-tube reactor, air can flow through the tubes, but also through the gaps in between the tubes and the reactor housing (Figure 1). In fact, the reactor forms a parallel flow system consisting of seven tubes, six very small gaps each surrounded by three tubes (further noted as 'internal gaps'), and six larger 'external gaps' each surrounded by two tubes and the reactor housing. Obviously, these flow channels are characterized by different flow rates geometries and photocatalytic surface areas, and an analytic mass transfer based model should be followed for each of them separately, using appropriate parameters. Since we could only control and measure the total flow rate through the reactor as a whole, the challenge was to determine the distribution of the total flow rate over the different parallel flow channels. The relative flow rates in parallel channels are established from the requirement that (1) the total flow rate is the sum of the flow rates in the individual channels and (2) the head loss in each channel be the same. Indeed, the head loss (or pressure drop) in each individual channel connected in parallel must be the same since $\Delta P = P_2 - P_1$ and P_1 and P_2 are the same for all the individual channels. For a system of tubes, internal and external gaps, this is expressed in terms of the Darcy-Weisbach equation as (eq. 3) [33]:

$$h_{L,t} = h_{L,ig} = h_{L,eg} \quad \longrightarrow \quad f_t \frac{L_t}{D_t}\frac{v_t^2}{2g} = f_{ig}\frac{L_{ig}}{D_{ig}}\frac{v_{ig}^2}{2g} = f_{eg}\frac{L_{eg}}{D_{eg}}\frac{v_{eg}^2}{2g} \qquad \text{(eq. 3)}$$

Where h is the head loss [m], f the friction factor, L and D the length [m] and hydraulic diameter of the channel [m], g the gravitational acceleration [m s^{-2}] and v the air speed in the channel [m s^{-1}] from which the flow rate can be determined. The subscripts t, ig and eg refer to the tubes, internal gaps and external gaps, respectively. From both requirements, a system of nonlinear equations was obtained that was solved using a Generalized Reduced Gradient (GRG) nonlinear solving method (Matlab). The flow distribution of the tubes, internal and external gaps was determined to be respectively 95.24 %, 0.14 % and 4.62 % for all flow rates (500 – 2000 mL min^{-1}). Based on this, the contribution of the internal and external gaps was assumed to be

negligible and the outlet concentration of a single tube ($C_{VOC,\infty,t,out}$) [mol m^{-3}] was derived by the following equation (eq. 4):

$$C_{VOC,\infty,t,out} = \frac{C_{VOC,\infty,out}}{7}\frac{G}{G_t} \quad \text{(eq. 4)}$$

Where $C_{VOC,\infty,out}$ is the concentration measured at the outlet of the multi-tube reactor [mol m^{-3}], G the total flow rate through the reactor [m^3 s^{-1}] and G_t the flow rate through a single tube [m^3 s^{-1}].

3.3.2 NTU_m-method

Zhang et al. proposed an analytic 'NTU_m-method' as an effective tool for designing and scaling up photocatalytic reactors [19]. In the approach, three parameters were introduced to reveal the VOC removal bottlenecks: (1) the 'ideal reaction number of mass transfer units' ($NTU_{m,ir}$), (2) the 'ideal reaction fractional conversion' (ε_{ir}) and (3) the 'reaction effectiveness' (η) [20,34]. Photocatalytic removal of VOCs is a combined effect of VOC transport towards the catalytic surface through convection and diffusion, establishing an adsorption-desorption equilibrium and the degradation of adsorbed VOCs at the photocatalyst surface. Depending on the operating conditions and the reactor geometry, the photocatalytic process can either be mass transfer limited or reaction limited (or both). In this work, the NTU_m-method was adapted for the multi-tube reactor. The mass conservation equation for an infinitely small section of a single tube, as shown in Figure 3, can be written as (eq. 5):

$$G_t \frac{\partial C_{VOC,\infty,t}(x)}{\partial x} dx = -j(x)p\,dx \quad \text{(eq. 5)}$$

With x the coordinate of the flow direction, $C_{VOC,\infty,t}$ the acetaldehyde bulk concentration [mol m^{-3}], p the length of the reaction surface perpendicular to the flow direction [m] (for a tube, this is the inner circumference of the circular cross section) and $j(x)$ [mol m^{-2} s^{-1}] the removal flux at the catalyst surface.

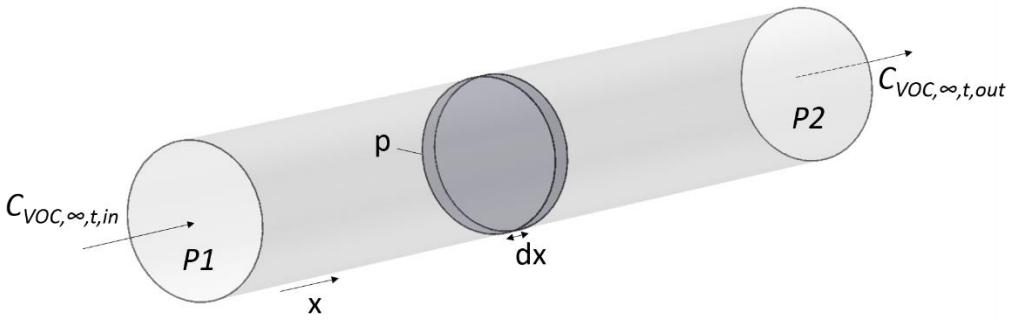

Figure 3: Schematic representation of a single tube, with *x* the coordinate of the flow direction, *p* the length of the reaction surface perpendicular to the flow direction. The infinitesimal volume element is indicated in dark gray.

The removal flux at the catalyst surface can also be written as (eq. 6):

$$j(x) = k_{app}(x)C_{VOC}(x) = h_{mass}(x)\left[C_{VOC,\infty,t}(x) - C_{VOC}(x)\right] \quad \text{(eq. 6)}$$

$$or\ j(x) = \frac{C_{VOC,\infty,t}(x)}{\frac{1}{h_{mass}(x)}+\frac{1}{k_{app}(x)}}$$

With h_{mass} the local convective mass transfer coefficient [m s^{-1}] which can be derived by using tabulated empirical expressions [35] (eq. 7)

$$Sh(x) = \frac{h_{mass}(x)D_h}{D} \quad \text{(eq. 7)}$$

with D_h [m] the hydraulic diameter (the inner diameter in case of a tube) and D [m^2 s^{-1}] the diffusion coefficient of the target VOC (in this case acetaldehyde) in air. Based on the analogy between heat and mass transfer, the Sherwood number is the equivalent of the Nusselt number. For fully developed laminar flow in a circular tube, the Sherwood and Nusselt numbers are independent of the Reynolds number: Sh = Nu = 3.66 [35]. Furthermore, as proposed by Zhang et al. (2003), a local 'total removing factor' K_t can be defined as (eq. 8) [20]:

$$K_t(x) = \frac{1}{\frac{1}{h_{mass}(x)}+\frac{1}{k_{app}(x)}} \quad \text{(eq. 8)}$$

Consequently, the mass conservation (eq. 5) for an infinitely small section of the tube can be rewritten as (eq. 9):

$$G_t \frac{\partial C_{VOC,\infty,t}(x)}{\partial x} dx = -K_t(x) C_{VOC,\infty,t}(x) p dx \quad \text{(eq. 9)}$$

When taking the entire length (L) of the tube into account, equation 9 can be integrated to yield (eq. 10):

$$C_{VOC,\infty,t,out} = C_{VOC,\infty,t,in} e^{\frac{-K_t A}{G_t}} \quad \text{(eq. 10)}$$

with $K_t = \int_0^L K_t(x) dx \Big/ L$ the average total removing factor over the entire length of photocatalytic surface and A the entire surface of the photocatalytic surface [m²]. In analogy with the number of transfer units for heat exchangers (NTU), the number of mass transfer units (NTU_m) for a photocatalytic tube can be defined as (eq. 11):

$$NTU_m = \frac{K_t A}{G_t} \quad \text{(eq. 11)}$$

Thus, the VOC removal efficiency of the photocatalytic tube can be expressed by the fractional conversion, ε, as shown in equation 12:

$$\varepsilon = \frac{C_{VOC,\infty,t,in} - C_{VOC,\infty,t,out}}{C_{VOC,\infty,t,in}} = 1 - e^{-NTU_m} \quad \text{(eq. 12)}$$

To acquire knowledge on the proportional contribution of the dimension of the tube to its performance, as compared to the impact of the photocatalytic surface activity, the ideal number of mass transfer units, the ideal fractional conversion and the reaction effectiveness, η, are introduced as given in eq. 13 and 14:

$$\varepsilon_{ideal} = 1 - e^{-NTU_{m,ideal}} \quad with \quad NTU_{m,ideal} = \frac{h_{mass} A}{G_t} \quad \text{(eq. 13)}$$

$$\eta = \frac{\varepsilon}{\varepsilon_{ideal}} \quad \text{(eq. 14)}$$

When considering ideal photocatalytic reaction conditions ($k_{app} \rightarrow \infty$) the system is completely controlled by mass transfer. In this case the total removing factor *Kt* equals h_{mass} (eq. 8). The ratio of fractional conversion and the hypothetical ideal fractional conversion (ideal photocatalytic reaction conditions) determines whether the system is mass-transfer or reaction

controlled. If η approaches 1 (k_{app} >> h_{mass}) the bottleneck of VOC removal is mass transfer. This implies that the performance can be enhanced by improving the geometric structure and dimension of the reactor. If η approaches 0 (h_{mass} >> k_{app}) the system is reaction-controlled and can be enhanced by improving reaction conditions, e.g. by increasing UV-irradiance.

3.3.3 Kinetic parameter estimation

In order to determine the kinetic parameters k_{LH} and K_L in the mass transfer based method. C_{VOC} has to be calculated using eq. 6 (restructured) (eq. 15):

$$C_{VOC} = \frac{C_{VOC,\infty,t}}{1+\frac{k_{app}}{h_{mass}}} = \frac{C_{VOC,\infty,t,in}+C_{VOC,\infty,t,out}}{2(1+\frac{k_{app}}{h_{mass}})} \quad \text{(eq. 15)}$$

Given the fact that C_{VOC} and $C_{VOC,\infty,t}$ vary over the length of the reactor, an average value for $C_{VOC,\infty,t}$ was calculated from the inlet and outlet experimental bulk concentrations. By plotting $1/k_{app}$ versus C_{VOC} for various experimental conditions (e.g. flow rates, inlet concentrations, …), a linear fit should be observed. k_{LH} can be derived from the inverse slope and K_L can be calculated from the intercept with the $1/k_{app}$-axis ($=k_{LH}^{-1} \cdot K_L^{-1}$) (eq. 1, restructured). A different k_{LH} will be obtained for various UV-irradiance conditions.

3.4 Extension of the mass transfer based model including radiation field modelling

An extension of the mass transfer based model is proposed in order to derive the kinetic parameters, which are not only independent of the pollutant concentration and fluid flow rate (as in 3.3) but also independent of the radiation field. An overview of the methodology is given in Figure 4.

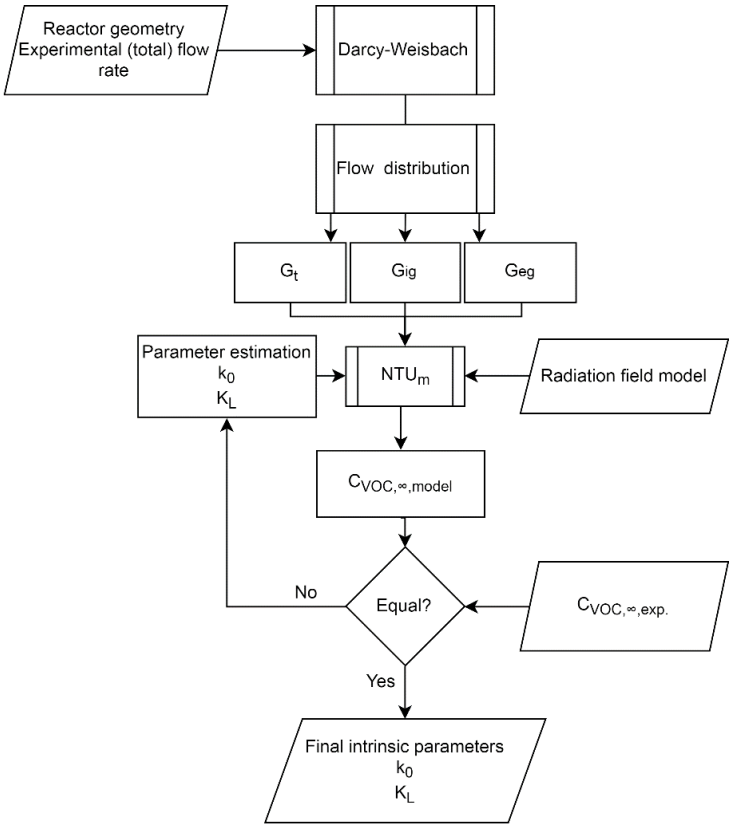

Figure 4: Overview of the methodology of the extended mass transfer based model including radiation field modelling

In the extended model, $C_{VOC,\infty,model}$ was calculated using the NTU_m method, applied on tubes (Figure 3), internal gaps (Figure 5a) and external gaps (Figure 5b).

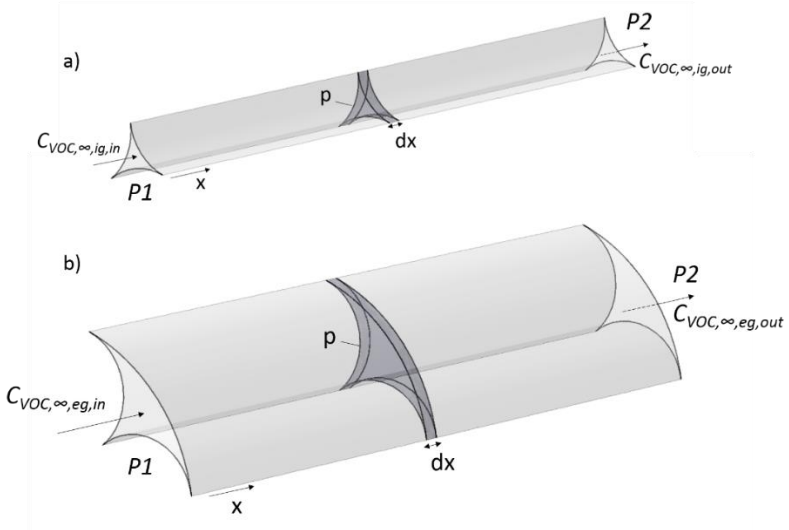

Figure 5: Schematic representation of an (a) internal and (b) external gap, with x the coordinate of the flow direction, p the length of the reaction surface perpendicular to the flow direction. The infinitesimal volume element is indicated in dark gray.

The Sherwood numbers were taken from tabulated empirical expressions [35]. As an assumption, internal and external gaps were regarded as isosceles triangular channels, for which Sherwood numbers are available, i.e. 3.11 and 2.68 for the internal and external gaps respectively. The photocatalytic surface areas of the individual channels were determined from a geometric analysis. By using the NTU_m-method for each of the channels separately, we can determine the removal efficiency and reaction effectiveness for each individual channel.

3.4.1 Radiation field modelling

The incident irradiation on the catalytic surface is a critical factor that determines the rate of conversion. In order to be able to derive the dependency of the incident irradiation on the LH rate constant k_{LH} (in other words, to determine the intrinsic empirical constant k_0 in eq. 2, which is independent of incident irradiation), the distribution of the incident irradiation in the multi-tube reactor should be measured, or at least be determined in some way. As measuring local light irradiation in a multi-tube reactor is not straightforward, we used a Comsol Multiphysics UV radiation field model, developed and tested in our previous work [23].

The radiation field model is based on the Ray Optics module of Comsol Multiphysics v5.3a which uses a ray trajectory approach allowing to simulate interactions of UV light with boundaries where refraction, reflection or absorption occurs. For a detailed description of the radiation field model, the reader is referred to Roegiers et al (2017) [23]. Despite the fact that the radiation field model provides an accurate spatial distribution of the UV light irradiation on all surfaces of the tubes and gaps (Roegiers et al., 2017), in the proposed method we assumed a single uniform value for the UV light irradiation for each individual channel. The latter was calculated as the surface averaged value of the spatial distribution for the particular channel. Given the symmetrical configuration of the reactor and the lamps, the UV irradiance on the

inner surfaces of the tubes, the internal gaps and the external gaps could be described with 7 different values for each irradiation condition, as shown in Figure 6.

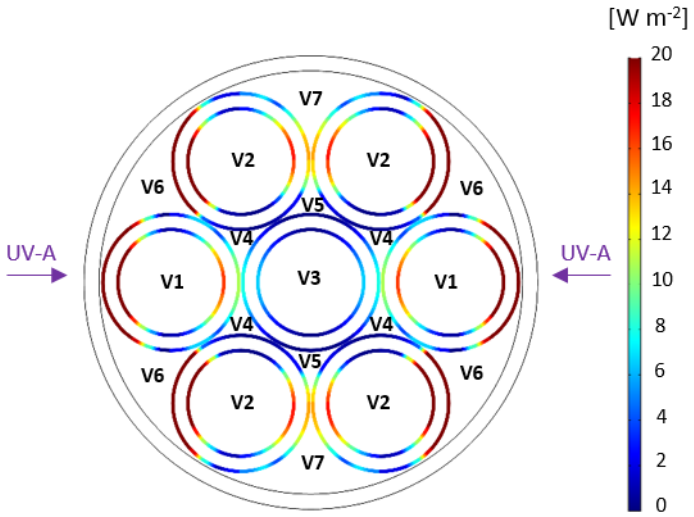

Figure 6: Values (V1-V7) of light irradiation, depending on the position within the multi-tube reactor. Two 8W UV-A fluorescent lamps are positioned on opposite sides of the reactor, at a distance of 20 mm (irradiation condition 1).

3.4.2 Intrinsic parameter estimation

Coupling the mass transfer based method with the radiation field model allows the determination of the intrinsic parameter k_0, using eq. 2. Assuming a uniform UV-irradiance on each glass tube, internal and external gap, $C_{VOC,\infty,t}$, $C_{VOC,\infty,ig}$ and $C_{VOC,\infty,eg}$ could be calculated for each individual channel by combining eq. 2 and eq. 10. The intrinsic empirical constant k_0 and the Langmuir adsorption constant K_L were derived using the Generalized Reduced Gradient (GRG) nonlinear solving method. Both constants were varied through a least-squares objective function (the squared difference of predicted and experimental outlet acetaldehyde concentrations). Initial values for k_0 and K_L were chosen in accordance with the results from Roegiers et al. (2017), i.e. 6.62×10^{-8} m² W^{-1} s^{-1} and 8764 m^3 mol^{-1}, respectively [23].

4. Results and discussion

4.1 Mass transfer based model (NTU_m-method) adapted for a multi-tube reactor

4.1.1. NTU_m-method

Experiments were conducted at three different irradiation conditions, corresponding to the distance of the UV lamps. For each condition, at least 15 individual experiments were carried out at 6 different flow rates (500, 750, 1000, 1250, 1500 and 2000 $cm^3\ min^{-1}$) and varying acetaldehyde inlet concentration. For each experiment, all relevant parameters to be used in, or obtained from the mass transfer based model were calculated. Because of the large amount of experiments, only a selection of the flow regimes (500-1250 $cm^3\ min^{-1}$) at the irradiation condition corresponding to the shortest distance (20 mm) of UV lamps is shown in Table 1. The values given in the table are for the tubes only, as gaps were excluded from the analysis. For a complete overview of the results for other conditions, the reader is referred to the supplementary files. Considering the low Reynolds numbers, the photocatalytic reactor is clearly operating in a laminar flow regime for all flow rates, which implicates a Sherwood number that is independent of the flow rate. Therefore, the mass transfer coefficient h_{mass} is constant for all experiments conducted in this work [35]. Obviously, the ideal number of mass transfer units ($NTU_{m,ideal}$) decreases as the flow rate increases, as evidenced by equation 13. For all conducted experiments, the ideal reaction fractional conversion (ε_{ir}), which represents the upper theoretical photocatalytic ability of the reactor, approaches 1. This indicates that the geometric structure of the reactor is optimal for the given experimental conditions [20].

Table 1: Experimental parameters of the mass transfer based model (NTU_m) for irradiation condition 1.

Parameter	Total volumetric flow rate ($cm^3\ min^{-1}$)			
	500	750	1000	1250
Maximum flow velocity (V_{tube} [$m\ s^{-1}$])	0.029	0.044	0.059	0.074
Maximum Reynolds number (Re)	13.72	20.57	27.43	34.29
Sherwood number (Sh)	4.36	4.36	4.36	4.36
h_{mass} [$m\ s^{-1}$]	0.0077	0.0077	0.0077	0.0077
$NTU_{m,ideal}$	36.04	24.03	18.02	14.42

ε_{ir}	1	1	1	1
ca. 27 ppmv inlet concentration				
Fractional conversion (ε)	0.94	0.92	0.81	0.73
Reaction effectiveness (η)	0.94	0.92	0.81	0.73
NTU_m	2.89	2.48	1.65	1.32
Average total removing factor (K_t)	6.19×10^{-4}	7.97×10^{-4}	7.01×10^{-4}	7.08×10^{-4}
Apparent rate constant (k_{app} [m s^{-1}])	6.73×10^{-4}	8.89×10^{-4}	7.81×10^{-4}	7.79×10^{-4}
ca. 35 ppmv inlet concentration				
Fractional conversion (ε)	0.93	0.87	0.69	0.60
Reaction effectiveness (η)	0.93	0.87	0.69	0.60
NTU_m	2.62	2.02	1.16	0.91
Average total removing factor (K_t)	5.62×10^{-4}	6.48×10^{-4}	4.96×10^{-4}	4.86×10^{-4}
Apparent rate constant (k_{app} [m s^{-1}])	6.06×10^{-4}	7.08×10^{-4}	5.30×10^{-4}	5.19×10^{-4}
ca. 42 ppmv inlet concentration				
Fractional conversion (ε)	0.93	0.74	0.59	0.50
Reaction effectiveness (η)	0.93	0.74	0.59	0.50
NTU_m	2.67	1.34	0.90	0.70
Average total removing factor (K_t)	5.73×10^{-4}	4.31×10^{-4}	3.84×10^{-4}	3.76×10^{-4}
Apparent rate constant (k_{app} [m s^{-1}])	6.19×10^{-4}	4.57×10^{-4}	4.04×10^{-4}	3.95×10^{-4}

The fractional conversion decreases as (1) the volumetric flow rate increases, (2) the inlet acetaldehyde concentration increases or (3) the incident light irradiance decreases (for the latter, the reader is referred to the supplementary files). Evidently, the fractional conversion ε and the reaction effectiveness η are equal since the ideal reaction fractional conversion ε_{ir} equals 1 (Eq. 14). The highest reaction effectiveness is obtained at the lowest inlet concentrations and flow rates. The reaction effectiveness approaches 1, indicating that the system is mass transfer-controlled. By increasing the flow rate under constant concentration conditions, the contribution of the photocatalytic reaction becomes more significant, as evidenced by a lower reaction

effectiveness. The same trend is observed when increasing the inlet concentration under a constant flow rate. At the highest concentration and flow rate a reaction effectiveness of 0.50 is obtained, which indicates a process controlled by both mass transfer and kinetic phenomena. At reduced irradiation under a constant flow rate and concentration, a shift towards more reaction-controlled conditions is observed (not shown in Table 1, the reader is referred to the supplementary files).

4.1.2. Kinetic parameter estimation

As mentioned in the methodology, by plotting $1/k_{app}$ versus C_{VOC} for all experiments, a linear fit should be observed. k_{LH} can be derived from the inverse slope and K_L can be calculated from the intercept with the $1/k_{app}$ -axis ($= k_{LH}^{-1}.K_L^{-1}$). The results are shown in Figure 7, for all three irradiation conditions and the derived kinetic parameters are listed in the overview Table 2.

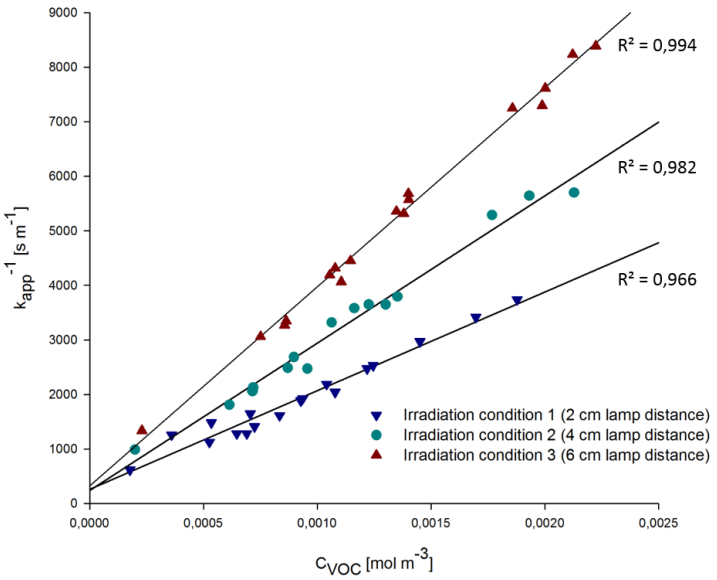

Figure 7: Plot of the inverse apparent reaction rate coefficient (k_{app}^{-1}) versus the acetaldehyde concentration in close proximity of the photocatalytic surface (C_{voc}) for three irradiation conditions.

For each irradiation condition, a linear fit was obtained with high R^2 values, respectively 0.966, 0.982 and 0.994 (Figure 7). The LH reaction constant k_{LH} increases with increasing irradiation which is in agreement with our earlier research, but for the Langmuir adsorption constant K_L,

no clear trend could be observed due to a sensitive variation of the intercept while finding the best fit with the experimental data.

Using the obtained kinetic parameters, the concentration $C_{VOC,\infty}$ over the reactor length can be determined for the tubes, internal and external gaps separately and based on the different flow regimes for these particular channels (Eq. 10). This was demonstrated for a randomly chosen experiment in Figure 8a. Obviously, the internal and external gaps, which account for a negligible part of the flow (0.14 % and 4.62 %, respectively), are capable of a total acetaldehyde removal within a few centimeters of the reactor inlet. For this particular experiment, about 75% of the acetaldehyde is mineralized at a length of 24 cm, whereas an extension of the reactor to 40 cm (indicated by the dotted line) would result in a complete removal under the given conditions, according to the NTU_m-model.

To validate the NTU_m-method, the predicted and experimental outlet concentrations are compared in Figure 8b for all experiments. Hereto, the overall outlet concentration of the reactor was calculated from the outlet concentrations and corresponding flow rates of the tubes, internal and external gaps. The agreement of the predicted and the experimental data is good as evidenced by a coefficient of determination of respectively 0.985, 0.991 and 0.998.

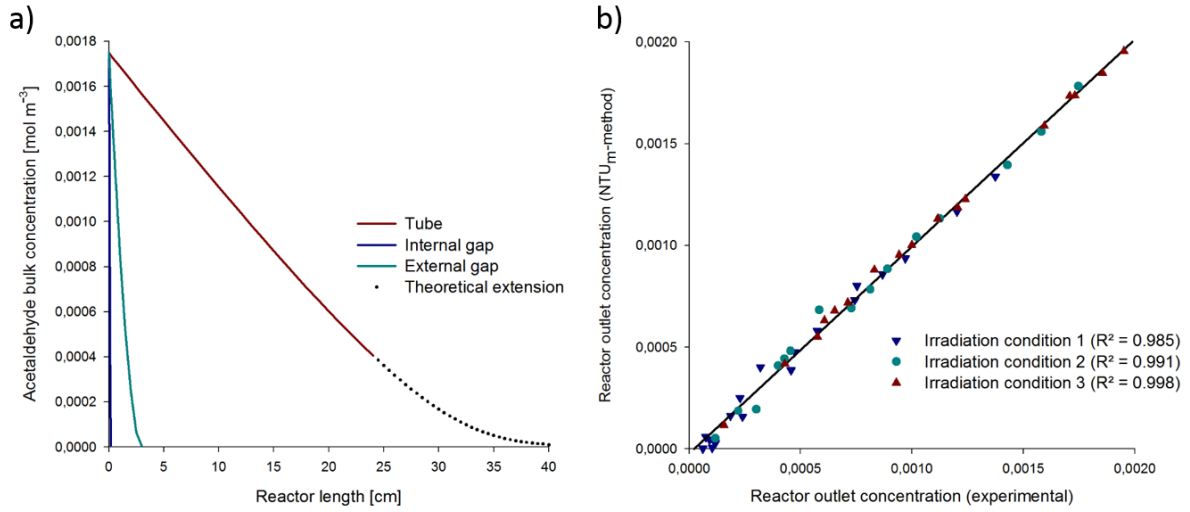

Figure 8: (a) Determined $C_{VOC,\infty}$ over the reactor length for the tubes, internal and external gaps separately for a randomly chosen experiment and (b) the predicted (NTU_m-method) reactor outlet concentrations versus the experimental reactor outlet concentrations for three irradiation conditions.

4.2 Extension of the mass transfer based model including radiation field modelling

Obviously, the adapted NTU_m-method is capable of providing accurate estimates for the Langmuir adsorption constant K_L and the Langmuir-Hinshelwood rate constant k_{LH} for a multi-tube reactor. However, it is important to emphasize that k_{LH} depends on the UV light irradiance and thus, is not an intrinsic parameter. The advantage of coupling the NTU_m-method with radiation field modelling lies in the possibility to derive a unique, intrinsic empirical constant k_0, valid for all irradiation conditions. This is shown in Table 2, where the kinetic parameters derived by the mass transfer based model and its extended version are summarized. For comparison, we included the Langmuir adsorption constant K_L and the irradiance independent kinetic parameter k_0, estimated by our earlier published CFD model [23] in the table. From the intrinsic empirical constant k_0 and the overall average incident UV irradiance (for the whole reactor, predicted by the radiation field model), the LH rate constants k_{LH} can be calculated from eq. 2 for each irradiation condition (last column for the extended model in Table 2). From the results, we can draw some interesting conclusions: Firstly, the empirical constant k_0 derived

from the extended mass transfer based model remains constant, regardless of the irradiation condition, which shows that this is really an intrinsic parameter. Besides, the value is in agreement with the intrinsic parameter derived from the earlier published CFD model [23], emphasizing the accuracy and reliability of the models. Secondly, there is a remarkable agreement between the LH reaction constants k_{LH} derived from the mass transfer based model and the values obtained indirectly from the extended model. Consequently, the LH reaction constant k_{LH} was calculated (eq. 2) for each individual channel, using the corresponding value for the empirical constant k_0 and the average incident UV irradiance for the specific channel (tubes, internal gaps and external gap), as determined from the methodology (Figure 9a). In the figure the radiation dependency of k_{LH} using the average value for empirical constant k_0, derived from all experiments is included (full line). The predicted and experimental reactor outlet concentrations were compared similarly as described in 4.1.2 and the model fits resulted in even better coefficients of determination, respectively 0.991, 0.994 and 0.998 (Figure 9b).

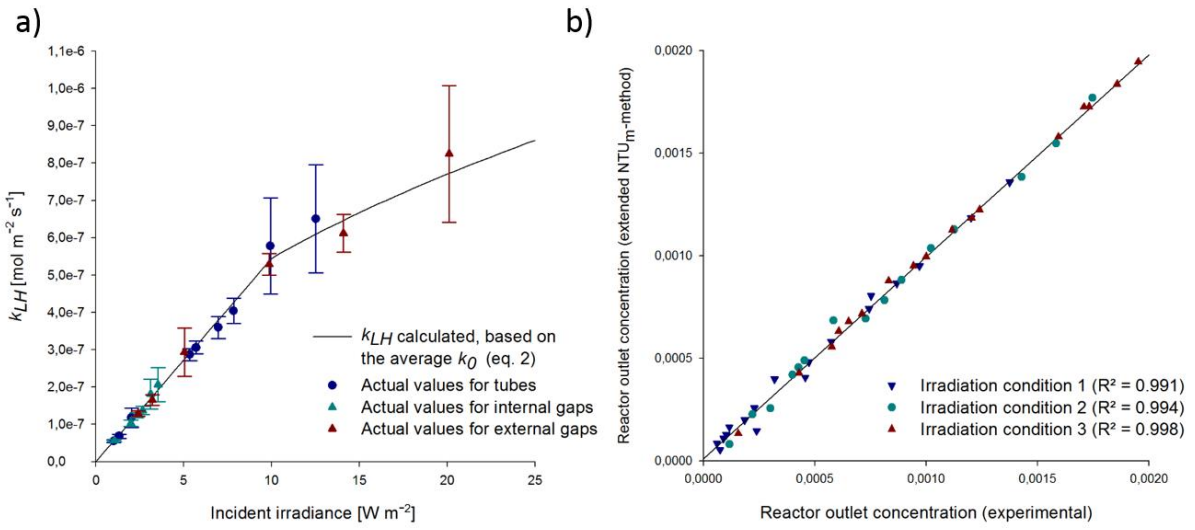

Figure 9: (a) The LH reaction constant (k_{LH}) versus the incident irradiance values within the multi-tube reactor for all irradiation conditions and (b) predicted (extended NTU$_m$-method) reactor outlet concentrations versus experimental reactor outlet concentrations for three irradiation conditions.

The derived intrinsic kinetic parameters are essential for scaling up purposes, since longer and wider reactor geometries result in complex UV light distributions and thus location dependent LH reaction constants. Combining an NTU_m-method with a radiation field model therefore provides the necessary tools for a thorough assessment of a multi-tube reactor, as well as a useful tool for reactor development and design optimization for indoor air purification.

Table 2: Overview of the kinetic parameters, derived by different models and for different irradiation conditions.

	K_L [$m^3\ mol^{-1}$]	k_0 [$m^2\ W^{-1}\ s^{-1}$]	k_{LH} [$mol\ m^{-2}\ s^{-1}$]
Mass transfer based model, irradiation condition 1	6836	NA	$5{,}53 \times 10^{-7}$
Mass transfer based model, irradiation condition 2	11242	NA	$3{,}70 \times 10^{-7}$
Mass transfer based model, irradiation condition 3	11160	NA	$2{,}74 \times 10^{-7}$
Extended model, irradiation condition 1 (avg 9.57 W m^{-2})	20733 ± 283	$5{,}82 \times 10^{-8} \pm 1.29 \times 10^{-9}$	$5{,}57 \times 10^{-7}$*
Extended model, irradiation condition 2 (avg 6.31 W m^{-2})	23895 ± 166	$5{,}16 \times 10^{-8} \pm 4.28 \times 10^{-9}$	3.25×10^{-7}*
Extended model, irradiation condition 3 (avg 4.83 W m^{-2})	21581 ± 43	$5{,}37 \times 10^{-8} \pm 2.98 \times 10^{-9}$	2.59×10^{-7}*
CFD model [23]	8764	6.62×10^{-8}	NA

*These values were calculated using the average of the incident UV irradiance of the tubes.

5. Conclusions

In this study, a mass transfer based model (NTU_m-method), proposed by Zhang et al (2003), was adapted for a multi-tube reactor in order to (1) provide insights in the reaction rate limiting behavior of the photocatalytic multi-tube reactor, through the reaction effectiveness parameter (η) for various experimental conditions and (2) derive photocatalytic related kinetic parameters, i.e. Langmuir adsorption constant K_L and LH reaction constant k_{LH}. However, k_{LH} depends on the incident UV light irradiation and thus cannot be regarded as an intrinsic parameter. We have shown that coupling the NTU_m-method with a radiation field model is capable of accurately deriving a unique intrinsic empirical constant k_0, emphasized by the agreement with earlier published parameter values, derived by a CFD approach. Therefore the method is directly applicable to other reactor configurations or irradiation conditions. Despite the outstanding

agreement between predicted and experimental reactor outlet concentrations for both methods, only the extended NTU_m-method was capable of deriving consistent values for the Langmuir adsorption constant K_L. Consequently, the proposed NTU_m-method coupled with radiation field modelling provides a convenient, accurate tool for estimating the kinetic parameters for a multi-tube reactor. Besides, the method can be used for reactor assessment, development and design.

6. Acknowledgement

J.V.W. acknowledges the Agentschap Innoveren & Ondernemen for a PhD fellowship.

7. References

[1] J. Auvinen, L.W. Ã, The influence of photocatalytic interior paints on indoor air quality, Atmos. Environ. 42 (2008) 4101–4112. doi:10.1016/j.atmosenv.2008.01.031.

[2] J. Mo, Y. Zhang, Q. Xu, Y. Zhu, J. Joaquin, R. Zhao, Determination and risk assessment of by-products resulting from photocatalytic oxidation of toluene, Appl. Catal. B Environ. 89 (2009) 570–576. doi:10.1016/j.apcatb.2009.01.015.

[3] F. Thevenet, L. Olivier, F. Batault, L. Sivachandiran, N. Locoge, Acetaldehyde adsorption on TiO2: Influence of NO2 preliminary adsorption, Chem. Eng. J. 281 (2015) 126–133. doi:10.1016/j.cej.2015.06.084.

[4] C. Marchand, B. Bulliot, S. Le Calvé, P. Mirabel, Aldehyde measurements in indoor environments in Strasbourg (France), Atmos. Environ. 40 (2006) 1336–1345. doi:10.1016/j.atmosenv.2005.10.027.

[5] Q. Liu, Y. Liu, M. Zhang, Personal exposure and source characteristics of carbonyl compounds and BTEXs within homes in Beijing, China, Build. Environ. 61 (2013) 210–216. doi:10.1016/j.buildenv.2012.12.014.

[6] B. Kartheuser, N. Costarramone, T. Pigot, S. Lacombe, NORMACAT project: normalized closed chamber tests for evaluation of photocatalytic VOC treatment in indoor air and formaldehyde determination., Environ. Sci. Pollut. Res. Int. 19 (2012) 3763–71. doi:10.1007/s11356-012-0797-0.

[7] C.H.H. Ao, S.C.C. Lee, Indoor air purification by photocatalyst TiO2 immobilized on an activated carbon filter installed in an air cleaner, Chem. Eng. Sci. 60 (2005) 103–109. doi:10.1016/j.ces.2004.01.073.

[8] M.A. Sidheswaran, H. Destaillats, D.P. Sullivan, S. Cohn, W.J. Fisk, Energy efficient indoor VOC air cleaning with activated carbon fiber (ACF) filters, Build. Environ. 47 (2012) 357–367. doi:10.1016/j.buildenv.2011.07.002.

[9] Y. Boyjoo, H. Sun, J. Liu, V.K. Pareek, S. Wang, A review on photocatalysis for air treatment: From catalyst development to reactor design, Chem. Eng. J. 310 (2017) 537–559. doi:10.1016/j.cej.2016.06.090.

[10] H. Destaillats, M. Sleiman, D.P. Sullivan, C. Jacquiod, J. Sablayrolles, L. Molins, Applied Catalysis B : Environmental Key parameters influencing the performance of photocatalytic oxidation (PCO) air purification under realistic indoor conditions, Appl. Catal. B Environ. 128 (2012) 159–170. doi:10.1016/j.apcatb.2012.03.014.

[11] O. Debono, F. Thévenet, P. Gravejat, V. Héquet, C. Raillard, L. Le Coq, et al., Gas phase photocatalytic oxidation of decane at ppb levels: Removal kinetics, reaction intermediates and carbon mass balance, J. Photochem. Photobiol. A. 258 (2013) 17–29. doi:10.1016/j.jphotochem.2013.02.022.

[12] Y. Paz, Application of TiO2 photocatalysis for air treatment: Patents' overview, Appl. Catal. B Environ. 99 (2010) 448–460.

[13] J. Mo, Y. Zhang, Q. Xu, J.J. Lamson, R. Zhao, Photocatalytic purification of volatile organic compounds in indoor air: A literature review, Atmos. Environ. 43 (2009) 2229–2246. doi:10.1016/j.atmosenv.2009.01.034.

[14] A.H. Mamaghani, F. Haghighat, C.S. Lee, Photocatalytic oxidation technology for indoor environment air purification: The state-of-the-art, Appl. Catal. B Environ. 203 (2017) 247–269. doi:10.1016/j.apcatb.2016.10.037.

[15] A.E. Cassano, O.M. Alfano, Reaction engineering of suspended solid heterogeneous photocatalytic reactors, Catal. Today. 58 (2000) 167–197. doi:10.1016/S0920-5861(00)00251-0.

[16] A.O. Ibhadon, I.M. Arabatzis, P. Falaras, D. Tsoukleris, The design and photoreaction kinetic modeling of a gas-phase titania foam packed bed reactor, Chem. Eng. J. 133 (2007) 317–323. doi:10.1016/j.cej.2007.02.018.

[17] S. Brosillon, L. Lhomme, C. Vallet, A. Bouzaza, D. Wolbert, Gas phase photocatalysis and liquid phase photocatalysis: Interdependence and influence of substrate concentration and photon flow on degradation reaction kinetics, Appl. Catal. B Environ. 78 (2008) 232–241. doi:10.1016/j.apcatb.2007.09.011.

[18] G. Li Puma, I. Salvadó-Estivill, T.N. Obee, S.O. Hay, Kinetics rate model of the photocatalytic oxidation of trichloroethylene in air over TiO2thin films, Sep. Purif. Technol. 67 (2009) 226–232. doi:10.1016/j.seppur.2009.03.011.

[19] Y. Zhang, R. Yang, R. Zhao, A model for analyzing the performance of photocatalytic air cleaner in removing volatile organic compounds, Atmos. Environ. 37 (2003) 3395–3399. doi:10.1016/S1352-2310(03)00357-1.

[20] R. Yang, Y.-P. Zhang, R.-Y. Zhao, An Improved Model for Analyzing the Performance of Photocatalytic Oxidation Reactors in Removing Volatile Organic Compounds and Its Application, J. Air Waste Manage. Assoc. 54 (2004) 1516–1524. doi:10.1080/10473289.2004.10471016.

[21] S.W. Verbruggen, S. Lenaerts, S. Denys, Analytic versus CFD approach for kinetic modeling of gas phase photocatalysis, Chem. Eng. J. 262 (2015) 1–8.

[22] J. van Walsem, J. Roegiers, B. Modde, S. Lenaerts, S. Denys, Integration of a photocatalytic multi-tube reactor for indoor air purification in HVAC systems : a feasibility study, Environ. Sci. Pollut. Res. (2018). doi:10.1007/s11356-018-2017-z.

[23] J. Roegiers, J. Van Walsem, S. Denys, CFD- and radiation field modeling of a gas phase photocatalytic multi-tube reactor, Chem. Eng. J. (2017) 1–33. doi:10.1016/J.CEJ.2018.01.047.

[24] J. van Walsem, S.W. Verbruggen, B. Modde, S. Lenaerts, S. Denys, CFD investigation of a multi-tube photocatalytic reactor in non-steady-state conditions, Chem. Eng. J. 304 (2016). doi:10.1016/j.cej.2016.07.028.

[25] Y. Chen, D.D. Dionysiou, TiO2 photocatalytic films on stainless steel: The role of Degussa P-25 in modified sol-gel methods, Appl. Catal. B Environ. 62 (2006) 255–264. doi:10.1016/j.apcatb.2005.07.017.

[26] Y. Chen, D.D. Dionysiou, A comparative study on physicochemical properties and photocatalytic behavior of macroporous TiO 2 -P25 composite films and macroporous TiO 2 films coated on stainless steel substrate, Appl. Catal. A. 317 (2007) 129–137. doi:10.1016/j.apcata.2006.10.025.

[27] T. Tytgat, B. Hauchecorne, M. Smits, S.W. Verbruggen, S. Lenaerts, Concept and Validation of a Fully Automated Photocatalytic Test Setup, J. Lab. Autom. 17 (2012). doi:10.1177/2211068211424554.

[28] S.W. Verbruggen, M. Keulemans, J. van Walsem, T. Tytgat, S. Lenaerts, S. Denys, CFD modeling of transient adsorption/desorption behavior in a gas phase photocatalytic fiber reactor, Chem. Eng. J. 292

(2016) 42–50. doi:10.1016/j.cej.2016.02.014.

[29] S.B. Kim, S.C. Hong, Kinetic study for photocatalytic degradation of volatile organic compounds in air using thin film TiO2 photocatalyst, Appl. Catal. B Environ. 35 (2002) 305–315. doi:10.1016/S0926-3373(01)00274-0.

[30] R. Yang, Y. Zhang, Q. Xu, J. Mo, A mass transfer based method for measuring the reaction coefficients of a photocatalyst, Atmos. Environ. 41 (2007) 1221–1229. doi:10.1016/j.atmosenv.2006.09.043.

[31] Y. Xu, C.H. Langford, Variation of Langmuir adsorption constant determined for TiO2-photocatalyzed degradation of acetophenone under different light intensity, J. Photochem. Photobiol. A Chem. 133 (2000) 67–71. doi:10.1016/S1010-6030(00)00220-3.

[32] Z. Wang, J. Liu, Y. Dai, W. Dong, S. Zhang, J. Chen, CFD modeling of a UV-LED photocatalytic odor abatement process in a continuous reactor, J. Hazard. Mater. 215–216 (2012) 25–31. doi:10.1016/j.jhazmat.2012.02.021.

[33] Y. Çengel, J.M. Cimbala, R.H. Turner, Fundamentals of Thermal-Fluid Sciences, 4th ed., McGraw-Hill, New York, 2012.

[34] J. Mo, Y. Zhang, R. Yang, Novel insight into VOC removal performance of photocatalytic oxidation reactors, Indoor Air. 15 (2005) 291–300. doi:10.1111/j.1600-0668.2005.00374.x.

[35] Y. Çengel, A.J. Ghajar, Heat and Mass Transfer: Fundamentals and Applications, 5th ed., McGraw-Hill, New York, 2014.